

# Pressure-induced enhancement of non-polar to polar transition temperature in metallic $\text{LiOsO}_3$

Esteban I. Paredes Aulestia,<sup>1</sup> Yiu Wing Cheung,<sup>1</sup> Yue-Wen Fang,<sup>2,\*</sup> Jianfeng He,<sup>3,4</sup>  
Kazunari Yamaura,<sup>3,4</sup> Kwing To Lai,<sup>1</sup> Swee K. Goh,<sup>1,5,†</sup> and Hanghui Chen<sup>2,6,‡</sup>

<sup>1</sup>*Department of Physics, The Chinese University of Hong Kong, Shatin, New Territories, Hong Kong, China*

<sup>2</sup>*NYU-ECNU Institute of Physics, NYU Shanghai, Shanghai, 200062, China*

<sup>3</sup>*Research Center for Functional Materials, National Institute for*

*Materials Science (NIMS), 1-1 Namiki, Tsukuba, Ibaraki 305-0044, Japan*

<sup>4</sup>*Graduate School of Chemical Sciences and Engineering, Hokkaido University,  
North 10 West 8, Kita-ku, Sapporo, Hokkaido 060-0810, Japan*

<sup>5</sup>*Shenzhen Research Institute, The Chinese University of Hong Kong, Shatin, New Territories, Hong Kong, China*

<sup>6</sup>*Department of Physics, New York University, New York 10003, USA*

(Dated: July 19, 2022)

$\text{LiOsO}_3$  undergoes a continuous transition from a centrosymmetric  $R\bar{3}c$  structure to a polar  $R3c$  structure at  $T_s = 140$  K. By combining transport measurements and first-principles calculations, we find that  $T_s$  is enhanced by applied pressure, and it reaches a value of  $\sim 250$  K at  $\sim 6.5$  GPa. The enhancement is due to the fact that the polar  $R3c$  structure of  $\text{LiOsO}_3$  has a smaller volume than the centrosymmetric  $R\bar{3}c$  structure. Pressure generically favors the structure with the smallest volume, and therefore further stabilizes the polar  $R3c$  structure over the  $R\bar{3}c$  structure, leading to the increase in  $T_s$ .

Ferroelectric materials are actively explored in both fundamental science and applied research for their potential industrial applications such as non-volatile memory devices, sensors and solar cells [1–9]. In ferroelectric materials, a continuous displacive phase transition from a centrosymmetric structure to a non-centrosymmetric structure occurs at Curie temperature  $T_C$ , below which a spontaneous polarization develops. Since itinerant electrons can effectively screen internal electric fields, it is a conventional wisdom that ferroelectric materials are insulators [10]. However, Anderson and Blount [11] argued that a second-order structural transition involving the formation of a polar axis and the disappearance of the inversion center, analogous to that of displacive ferroelectrics, may result in a ‘ferroelectric-like metal’. Pugioni *et al.* [12] further deduced that such transition may be a result of the electrons at the Fermi level that are only weakly coupled to the soft phonon mode that drives the second-order phase transition into the polar structure. Recently, Shi *et al.* [10] showed clear evidence of a polar metallic state in  $\text{LiOsO}_3$ , which has stimulated many further experimental and theoretical works [12–21]. At a critical temperature  $T_s = 140$  K,  $\text{LiOsO}_3$  undergoes a structural transition from centrosymmetric  $R\bar{3}c$  (space group 167) at high temperature to a polar, non-centrosymmetric  $R3c$  (space group 161) below  $T_s$ . This structural transition is analogous to that in  $\text{LiNbO}_3$ , which is a well-known ferroelectric compound ( $T_C = 1483$  K [22]) and thus the insulating equivalent of  $\text{LiOsO}_3$ . The heat capacity data displays a broad peak at  $T_s$  without any thermal hysteresis, which is characteristic of a second-order phase transition. The temperature dependence ( $T$ ) of the electrical resistivity ( $\rho$ ) exhibits a positive  $d\rho/dT$  from 300 K to 2 K, indicating the metallic nature of the system over the entire temperature range studied.

The polar properties of both conventional (insulating) ferroelectrics and polar metals can be tuned by external factors such as atomic substitution, chemical ordering and pressure. In a classical paper, Samara *et al.* [23] showed that hydrostatic pressure decreases the transition temperature in conventional ferroelectrics and ultimately destabilizes the polarization. That is because pressure increases short-range interactions much more rapidly than long-range interactions and as a result, the harmonic soft-mode frequency becomes less negative with increasing pressure [24]. Such pressure-induced suppression of ferroelectricity is observed in  $\text{BaTiO}_3$  [25–27] and  $\text{BiFeO}_3$  [28]. On the other hand, negative pressure is found to increase ferroelectric Curie temperature and polarization in free-standing  $\text{PbTiO}_3$  particles [29].

In this work, we combine transport measurements up to 6.5 GPa and first-principles calculations to show that hydrostatic (positive) pressure can enhance the transition temperature of  $\text{LiOsO}_3$ , in contrast to conventional ferroelectrics. Recently, a novel ‘cubic Dirac point’ is predicted in the  $R\bar{3}c$  phase, which transforms into three mutually crossed nodal rings in the  $R3c$  phase [21]. Thus, the prospect of stabilizing the nodal rings at elevated temperature is attractive. The pressure-induced enhancement of the transition temperature is due to the fact that the volume of the non-centrosymmetric structure ( $R3c$ ) is smaller than that of the centrosymmetric structure ( $R\bar{3}c$ ). Pressure generically favors the structure with the smallest volume and therefore with pressure, the polar  $R3c$  structure of  $\text{LiOsO}_3$  becomes more stable over the  $R\bar{3}c$  structure and  $T_s$  increases. The same analysis can also be applied to conventional ferroelectrics, which predicts an increase of  $T_C$  and polarization in  $\text{LiNbO}_3$  and  $\text{ZnSnO}_3$  with pressure [30].

Single crystals of  $\text{LiOsO}_3$  were synthesized by a high-pressure solid state reaction as described elsewhere [10].

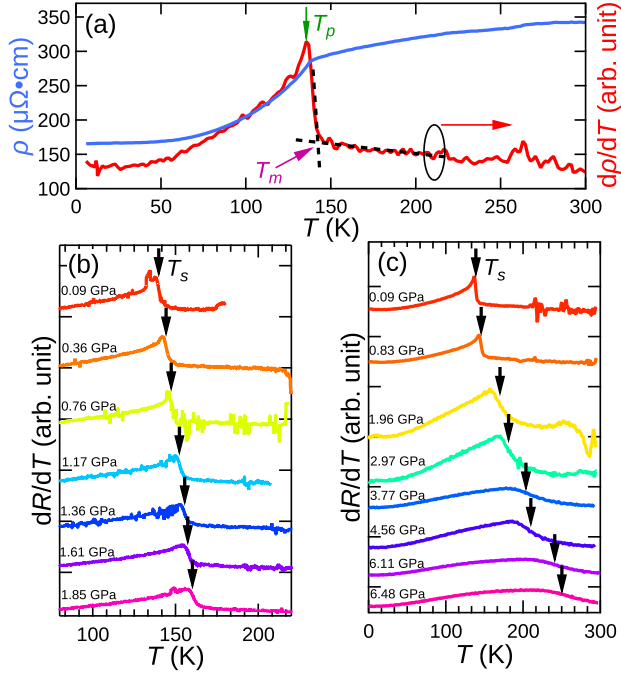


FIG. 1. (a) Temperature dependence of  $\rho(T)$  and  $d\rho/dT$  of LiOsO<sub>3</sub> at ambient pressure. The definitions of  $T_p$  and  $T_m$  are shown. (b) Temperature dependence of the first derivative of resistance  $dR/dT$  of LiOsO<sub>3</sub> at different pressures provided by the clamp cell. (c) Temperature dependence of  $dR/dT$  of LiOsO<sub>3</sub> at different pressures in the anvil cell. The vertical arrows in (b) and (c) mark  $T_s$ .

Electrical resistance measurements were conducted using a standard four-probe technique. The electrodes were made with gold wires and silver paste (Dupont 6838) on the polished surface of the single crystals. High-pressure experiments were performed in a piston-cylinder clamp cell and a miniature moissanite anvil cell. The clamp cell provides a higher pressure-resolution than the anvil cell, but with a smaller pressure range. Two pieces of single crystals from the same batch were used, one in each pressure cell. The pressure achieved in the clamp cell was estimated by the zero-field superconducting transition of a piece of Pb placed near the sample, while the pressure value inside the anvil cell was determined by ruby fluorescence spectroscopy at room temperature. Glycerin was used as the pressure transmitting medium for both types of pressure cells. Low-temperature environment down to 2 K was provided by a Physical Property Measurement System (PPMS) made by Quantum Design.

Density functional theory (DFT) calculations within the *ab initio* plane-wave approach, as implemented in the Vienna Ab-initio Simulation Package (VASP) [31, 32], were performed. A plane wave basis set and projector-augmented wave method [33] were employed. PBEsol, a revised Perdew-Burke-Ernzerhof generalized gradient approximation which improved equilibrium properties of densely-packed solids [34], was used as the exchange-

correlation functional. The cutoff energy was set as 600 eV and a  $12 \times 12 \times 12$  Monkhorst-Pack grid was used to sample the Brillouin zone. The threshold of energy convergence was  $10^{-7}$  eV. In the structural relaxation, each Hellmann-Feynman force component was smaller than  $10^{-3}$  eV/Å and the stress tensor was smaller than 0.1 GPa. The phonon frequencies at  $\Gamma$  point of centrosymmetric  $R\bar{3}c$  LiOsO<sub>3</sub> were computed via density functional perturbation theory method [35].

In LiOsO<sub>3</sub>, this resistance exhibits a kink at  $T_s$ . Therefore, the metallic nature of LiOsO<sub>3</sub> offers an elegant method to follow  $T_s$  under pressure using a simple resistance ( $R$ ) measurement, as opposed to the more elaborate dielectric constant measurement for tracking  $T_C$  in conventional ferroelectric materials. Figure 1(a) shows the temperature dependence of electrical resistivity  $\rho(T)$  and its temperature derivative  $d\rho/dT$  at ambient pressure.  $\rho(T)$  shows a metallic behavior over the entire temperature range measured, and exhibits a kink at 140 K, consistent with the previous result [10].  $d\rho/dT$  shows a rapid increase near the kink. We define  $T_m$  as the temperature at which  $d\rho/dT$  begins to rise rapidly, and  $T_p$  as the temperature when  $d\rho/dT$  peaks (see Fig. 1(a)). The transition temperature  $T_s$  is the average between  $T_m$  and  $T_p$ . At low pressures, when the kink is pronounced,  $T_m$  is very close to  $T_p$ . Figure 1(b) displays the temperature dependence of the first derivative of resistance  $dR/dT$  at different pressures in the clamp cell. With pressure,  $T_s$  seemingly experiences an enhancement. To investigate the behavior of  $T_s$  at higher pressures, the anvil cell data is used, and the temperature dependence of  $dR/dT$  is plotted in Fig. 1(c). At 6.48 GPa, the highest pressure of this experiment, the peak-like anomaly in  $dR/dT$  is significantly broadened. Using  $T_p$  and  $T_m$ ,  $T_s$  is determined to be  $(250 \pm 44)$  K at 6.48 GPa. The  $R(T)$  curves, from which the  $dR/dT$  are constructed, are presented in the supplementary material.

Figure 2(a) summarizes the structural transition temperatures  $T_s(P)$  at different applied pressures obtained by the clamp cell and the anvil cell techniques. At the low pressure region ( $\leq 2$  GPa),  $T_s(P)$  obtained via the clamp cell overlaps with that obtained via the anvil cell, indicating that the data from both techniques are consistent with each other. At the high pressure region ( $> 2$  GPa),  $T_s(P)$  continues to increase. The overall  $T_s(P)$  is linear with a large slope of  $\sim 17.54$  K/GPa. Therefore, our experimental results unambiguously demonstrate the enhanced stability of the polar phase.

DFT calculations were performed to understand the observed pressure effect on  $T_s$  of LiOsO<sub>3</sub>. Figure 2(b1) and (b2) show the fully relaxed centrosymmetric structure ( $R\bar{3}c$ , non-polar) and the non-centrosymmetric structure ( $R3c$ , polar) of LiOsO<sub>3</sub>, respectively, obtained from DFT-PBEsol calculations at ambient conditions. In the  $R\bar{3}c$  structure, the Os atom is located at the center of the oxygen octahedron, which is also the symmetric center of the two Li ions. In the  $R3c$  structure, the inversion symmetry is broken owing to the dominant contribu-

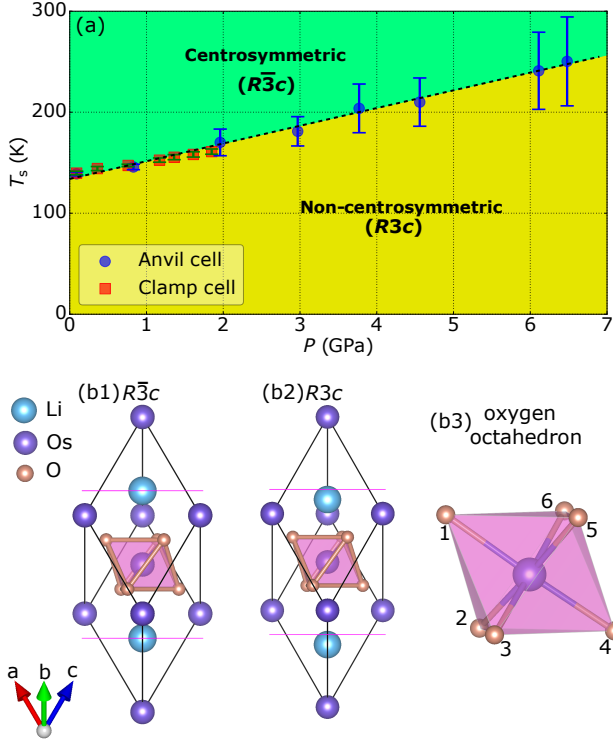


FIG. 2. (a) Pressure dependence of  $T_s$ . The blue dots (red squares) with blue (red) error bars represent the data obtained via the anvil (clamp) cell technique. The dashed straight line is obtained by a least-squares fitting to the anvil cell data. (b) Crystal structures of (b1) centrosymmetric ( $R\bar{3}c$ ) and (b2) non-centrosymmetric ( $R3c$ ) LiOsO<sub>3</sub>. The magenta horizontal lines representing the (111) planes across the high symmetry points  $(1/4, 1/4, 1/4)$  and  $(3/4, 3/4, 3/4)$  are shown to guide the eyes. Here,  $(1/4, 1/4, 1/4)$  and  $(3/4, 3/4, 3/4)$  are fractional coordinates that are parallel to the crystallographic axes. (b3) An OsO<sub>6</sub> oxygen octahedron.

tion from Li displacements and a much smaller contribution from Os off-center displacements [20]. Figure 2(b3) displays the OsO<sub>6</sub> octahedron in LiOsO<sub>3</sub>. In both polar and non-polar structures, the three Os–O bond angles O1–Os–O4, O2–Os–O5 and O3–Os–O6 are identical, protected by the  $R3c$  and  $R\bar{3}c$  symmetries, respectively. Hence we only focus on the O1–Os–O4 bond angle. This bond angle is 180° when protected by  $R\bar{3}c$  symmetry but deviates from 180° in the  $R3c$  symmetry. Therefore, the bond angle is a good structural parameter quantifying the structural change with respect to  $R\bar{3}c$  structure. The experimental [10] and theoretical O–Os–O bond angles, average Os–O bond lengths and volumes of both structures at ambient conditions are tabulated in Table I, showing a good agreement between theory and experiment for both  $R\bar{3}c$  and  $R3c$  symmetries. More importantly, the volume of polar structure ( $R3c$ ) is smaller than that of non-polar structure ( $R\bar{3}c$ ). This will play an essential role in understanding the enhancement of  $T_s$  under pressure.

TABLE I. Structural parameters for  $R\bar{3}c$  and  $R3c$  structures of LiOsO<sub>3</sub> obtained from DFT calculations, compared to experimental values [10] shown in brackets. The predicted  $Pbnm$  structure which is next to  $R\bar{3}c$  LiOsO<sub>3</sub> in energy at 0 GPa is also shown as a comparison, more details on  $Pbnm$  phase can be found in the supplementary material. The volume is normalized to per formula unit of LiOsO<sub>3</sub>, the bond angle corresponds to angle O1–Os–O4 in Fig. 2(b3), and the bond length corresponds to the average length of O–Os in Fig. 2(b3).

structural parameter	space group		
	$R\bar{3}c$	$R3c$	$Pbnm$
volume (Å <sup>3</sup> )	49.12 (48.90)	48.71 (48.65)	48.45
bond angle (°)	180 (180)	178.03 (176.84)	180
bond length (Å)	1.946 (1.944)	1.947 (1.944)	1.946

The left axis in Fig. 3 shows the pressure dependence of the lowest phonon frequency at  $\Gamma$  point of the non-polar  $R\bar{3}c$  LiOsO<sub>3</sub> at zero temperature. The phonon frequency is found to be imaginary and its magnitude increases with pressure, indicating that the non-polar  $R\bar{3}c$  structure is unstable and pressure enhances the instability of the zone-center phonon mode. On the other hand, the right axis in Fig. 3 shows the pressure dependence of the O1–Os–O4 bond angle of polar  $R3c$  LiOsO<sub>3</sub>. As pressure increases, the bond angle decreases and deviates further from the ideal 180°. This shows that applying pressure can enhance the polar nature of  $R3c$  LiOsO<sub>3</sub>. Therefore, both results show that external pressure not only destabilizes non-polar  $R\bar{3}c$  LiOsO<sub>3</sub>, but also renders  $R3c$  LiOsO<sub>3</sub> more polar.

To understand why pressure favors the polar structure  $R3c$  over the non-polar structure  $R\bar{3}c$ , zero-temperature thermodynamic functions of LiOsO<sub>3</sub> were computed via DFT calculations. Figure 4(a) shows the zero-temperature enthalpy  $H$  of LiOsO<sub>3</sub> in three structures with the lowest enthalpy,  $R3c$ ,  $R\bar{3}c$  and  $Pbnm$ , based on

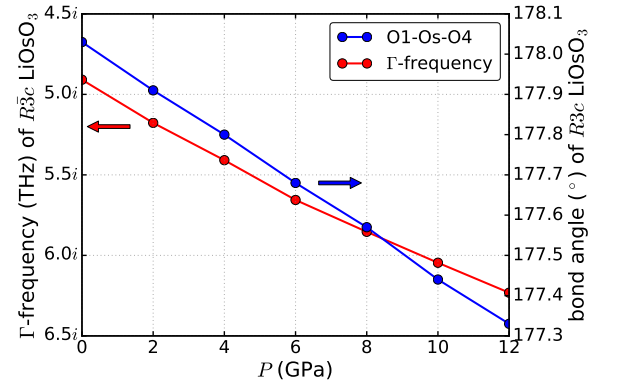


FIG. 3. (Left vertical axis) Lowest zone-center phonon frequency of  $R3c$  LiOsO<sub>3</sub> as a function of pressure. (Right vertical axis) O1–Os–O4 bond angle of  $R3c$  LiOsO<sub>3</sub> as a function of pressure. The O1–Os–O4 bond angle is shown in Fig. 2(b3).

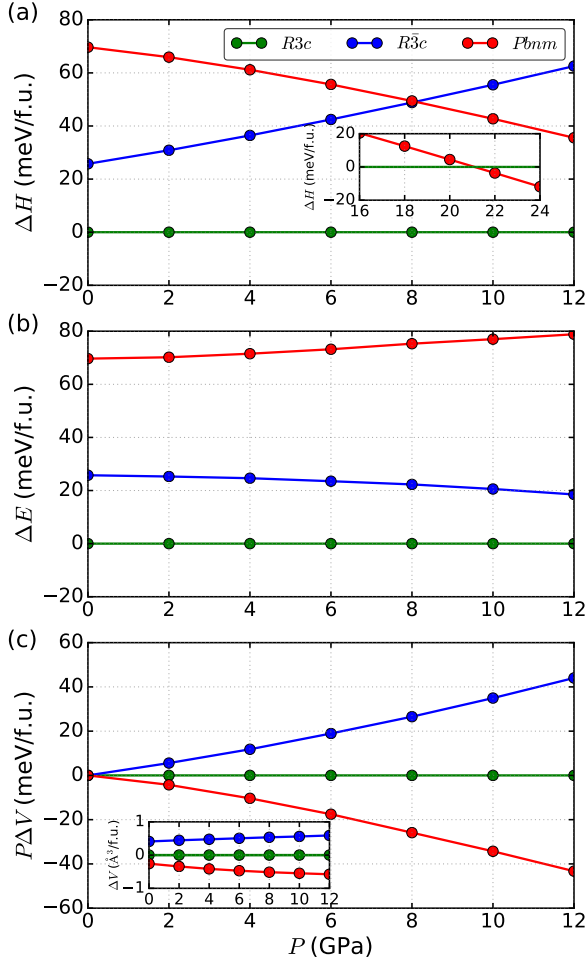


FIG. 4. Zero-temperature thermodynamic properties of LiOsO<sub>3</sub> under pressure. (a) Enthalpy difference  $\Delta H$  between  $R3c$  and other structures. The inset in (a) shows the  $\Delta H$  under 16 ~ 24 GPa. (b) Energy difference  $\Delta E$  between  $R3c$  and other structures. (c) Pressure times volume difference  $P\Delta V$  between  $R3c$  and other structures. The inset in (c) shows  $\Delta V$  between  $R3c$  and other structures. The green, blue and red symbols correspond to  $R3c$ ,  $R3c$  and  $Pbnm$  structures, respectively.  $R3c$  is chosen as the reference state.

our structure search study (see the supplementary material). For all pressures, the enthalpy of the  $R3c$  structure is used as the reference. The blue and green symbols in Fig. 4(a) show that the  $R3c$  structure is more stable than the  $R3c$  structure, and pressure increases the stability of the  $R3c$  structure over the  $R3c$  structure, which is consistent with the trend shown in Fig. 3. On the other hand, though the  $Pbnm$  structure has higher energy than the  $R3c$  structure at ambient pressure, applying pressure reduces the enthalpy difference between  $Pbnm$  and  $R3c$  structures, and eventually stabilizes the  $Pbnm$  structure over the  $R3c$  structure at about 21 GPa. It is known that the ferroelectric transition temperature is proportional to the energy difference between the polar structure and the corresponding high-symmetry non-polar structure [36].

Under pressure, enthalpy replaces energy as the thermodynamic function. Therefore, the increasing enthalpy difference between  $R3c$  and  $R3c$  structures leads to the enhancement of  $T_s$ , which is consistent with our experiment. Furthermore, the enthalpy difference between  $R3c$  and  $R3c$  structures, and the Li displacement squared in  $R3c$  LiOsO<sub>3</sub> (see the supplementary material) almost increase linearly with pressure, which is also consistent with the experimentally observed linear  $T_s(P)$  displayed in Fig. 2(a).

Using the relation  $H = E + PV$ , the total energy  $E$  and  $PV$  for different structures of LiOsO<sub>3</sub>, with respect to  $R3c$ , are illustrated in Figs. 4(b) and (c), respectively. As pressure increases,  $\Delta E$  only changes slightly. Moreover, the pressure dependence of  $\Delta E$  is opposite to that of  $\Delta H$ . This indicates that the pressure dependence of  $\Delta H$  is dominated by  $P\Delta V$ . As the inset of Fig. 4(c) shows, the volume of the polar  $R3c$  LiOsO<sub>3</sub> is always smaller than that of the non-polar  $R3c$  LiOsO<sub>3</sub>, and  $\Delta V$  is almost a constant within the pressure range we study. As a result,  $P\Delta V$  increases linearly with  $P$  and so does  $\Delta H$  because  $\Delta E$  has weak dependence on  $P$ .

Figure 4 provides a simple criterion to predict the pressure effects on polar metals. If the volume of the polar structure is smaller than that of the non-polar structure at ambient pressure, pressure enhances the polar properties (increasing  $T_s$  and polar distortions). Conversely, if the volume of polar structure is larger, pressure will suppress the polar properties (decreasing  $T_s$ ). This simple criterion can also be applied to conventional insulating ferroelectrics (see supplementary material). For example, LiNbO<sub>3</sub> and ZnSnO<sub>3</sub> belong to the former class ( $V(\text{polar}) < V(\text{non-polar})$ ), which have been predicted to feature a pressure-enhanced ground state polarization and  $T_C$  [30, 37]. On the other hand, BaTiO<sub>3</sub> and BiFeO<sub>3</sub> belong to the latter class ( $V(\text{polar}) > V(\text{non-polar})$ ), and it has been observed that pressure reduces the polarization and eventually destabilizes the ferroelectric ground state [25–28].

Note that the enhancement of  $T_s$  via pressure in LiOsO<sub>3</sub> will be thwarted by the stabilization of a different structure. As Fig. 4(a) shows, the non-polar  $Pbnm$  structure becomes more stable than the non-polar  $R3c$  structure above 8 GPa, and becomes more stable than the polar  $R3c$  structure above 21 GPa. As a conservative estimation using the linear pressure dependence,  $T_s$  in LiOsO<sub>3</sub> can be enhanced up to ~274 K at 8 GPa. The robustness of our conclusions is also tested by considering the effects of Hubbard  $U$ , spin-orbital coupling (SOC) and possible magnetic ordering. The results from DFT+ $U$ , DFT+SOC and DFT+ $U$ +SOC calculations all agree qualitatively with Fig. 4(a) (see the supplementary material for details).

In summary, the pressure dependence of structural transition temperature  $T_s$  in polar metal LiOsO<sub>3</sub> was measured up to ~ 6.5 GPa.  $T_s$  increases linearly under pressure, reaching 250 K at ~ 6.5 GPa. The experimental result is corroborated by first-principle

calculations which show that pressure further stabilizes the polar  $R3c$  phase over the centrosymmetric  $R\bar{3}c$  phase and enhances the polar properties in the  $R3c$  structure. The enhancement of  $T_s$  arises from the fact that the volume of the polar  $R3c$  structure is smaller than that of the non-polar  $R\bar{3}c$  structure, and pressure generically favors the structure with the smallest volume. This criterion can also be applied to insulating ferroelectrics, which predicts pressure increases polarization and  $T_C$  in  $\text{ZnSnO}_3$  and  $\text{LiNbO}_3$  [30].

See supplementary material for the method for determining  $T_s$  and further details on theoretical investigations including the structure search and the

connection between the volume and oxygen octahedra rotations.

We acknowledge support from Research Grants Council of Hong Kong (ECS/24300214, GRF/14300117), CUHK Direct Grant (4053223, 4053299), National Natural Science Foundation of China (11774236, 11504310), the Seed Grants of NYU-ECNU Joint Research Institutes, the JSPS KAKENHI (JP15K14133 and JP16H04501), and JSPS Bilateral Open Partnership Joint Research Projects. We thank Sheng Wang for helpful discussions on crystal structure prediction. Extreme Science and Engineering Discovery Environment (XSEDE) provides computational resources.

- 
- \* Present address: Department of Materials Science and Engineering, Kyoto University, Kyoto 606-8501, Japan  
<sup>†</sup> skgoh@phy.cuhk.edu.hk  
<sup>‡</sup> hanghui.chen@nyu.edu
- [1] F. Li, D. Lin, Z. Chen, Z. Cheng, J. Wang, C. Li, Z. Xu, Q. Huang, X. Liao, L.-Q. Chen, *et al.*, *Nat. Mater.* **17**, 349 (2018).
  - [2] V. Garcia and M. Bibes, *Nat. Commun.* **5**, 4289 (2014).
  - [3] Y.-W. Fang, C. A. Fisher, A. Kuwabara, X.-W. Shen, T. Ogawa, H. Moriwake, R. Huang, and C.-G. Duan, *Phys. Rev. B* **95**, 014111 (2017).
  - [4] Y.-H. Hsieh, F. Xue, T. Yang, H.-J. Liu, Y. Zhu, Y.-C. Chen, Q. Zhan, C.-G. Duan, L.-Q. Chen, Q. He, *et al.*, *Nat. Commun.* **7**, 13199 (2016).
  - [5] Y. Qi, S. Liu, A. M. Lindenberg, and A. M. Rappe, *Phys. Rev. Lett.* **120**, 055901 (2018).
  - [6] Z. Lu, C. Serrao, A. I. Khan, J. D. Clarkson, J. C. Wong, R. Ramesh, and S. Salahuddin, *Appl. Phys. Lett.* **112**, 043107 (2018).
  - [7] X. Liu, E. Y. Tsybal, and K. M. Rabe, *Phys. Rev. B* **97**, 094107 (2018).
  - [8] M. Nakamura, S. Horiuchi, F. Kagawa, N. Ogawa, T. Kurumaji, Y. Tokura, and M. Kawasaki, *Nat. Commun.* **8**, 281 (2017).
  - [9] H. Chen and A. Millis, *Scientific Reports* **7**, 6142 (2017).
  - [10] Y. Shi, Y. Guo, X. Wang, A. J. Princep, D. Khalyavin, P. Manuel, Y. Michiue, A. Sato, K. Tsuda, S. Yu, M. Arai, Y. Shirako, M. Akaogi, N. Wang, K. Yamaura, and A. T. Boothroyd, *Nat. Mater.* **12**, 1024 (2013).
  - [11] P. W. Anderson and E. I. Blount, *Phys. Rev. Lett.* **14**, 217 (1965).
  - [12] D. Puggioni and J. M. Rondinelli, *Nat. Commun.* **5**, 3432 (2014).
  - [13] I. L. Vecchio, G. Giovannetti, M. Autore, P. D. Pietro, A. Perucchi, J. He, K. Yamaura, M. Capone, and S. Lupi, *Phys. Rev. B* **93**, 161113 (2016).
  - [14] T. Kim, D. Puggioni, Y. Yuan, L. Xie, H. Zhou, N. Campbell, P. Ryan, Y. Choi, J.-W. Kim, J. Patzner, *et al.*, *Nature* **533**, 68 (2016).
  - [15] D. Varjas, A. G. Grushin, R. Ilan, and J. E. Moore, *Phys. Rev. Lett.* **117**, 257601 (2016).
  - [16] H. J. Xiang, *Phys. Rev. B* **90**, 094108 (2014).
  - [17] H. M. Liu, Y. P. Du, Y. L. Xie, J.-M. Liu, C.-G. Duan, and X. Wan, *Phys. Rev. B* **91**, 064104 (2015).
  - [18] D. Puggioni, G. Giovannetti, M. Capone, and J. M. Rondinelli, *Phys. Rev. Lett.* **115**, 087202 (2015).
  - [19] A. Filippetti, V. Fiorentini, F. Ricci, P. Delugas, and J. Íñiguez, *Nat. Commun.* **7**, 11211 (2016).
  - [20] G. Giovannetti and M. Capone, *Phys. Rev. B* **90**, 195113 (2014).
  - [21] W. C. Yu, X. Zhou, F.-C. Chuang, S. A. Yang, H. Lin, and A. Bansil, *Phys. Rev. Materials* **2**, 051201 (2018).
  - [22] K. Nassau and H. J. Levinstein, *Appl. Phys. Lett.* **7**, 69 (1965).
  - [23] G. A. Samara, T. Sakudo, and K. Yoshimitsu, *Phys. Rev. Lett.* **35**, 1767 (1975).
  - [24] I. A. Kornev and L. Bellaiche, *Phase Transitions* **80**, 385 (2007).
  - [25] T. Ishidate, S. Abe, H. Takahashi, and N. Môri, *Phys. Rev. Lett.* **78**, 2397 (1997).
  - [26] J. L. Zhu, S. Lin, S. M. Feng, F. Y. Li, L. J. Wang, C. Q. Jin, X. H. Wang, and L. T. Li, *J. Phys.: Conf. Ser.* **121**, 162005 (2008).
  - [27] E. Bousquet and P. Ghosez, *Phys. Rev. B* **74**, 180101 (2006).
  - [28] R. Haumont, P. Bouvier, A. Pashkin, K. Rabia, S. Frank, B. Dkhil, W. A. Crichton, C. A. Kuntscher, and J. Kreisel, *Phys. Rev. B* **79**, 184110 (2009).
  - [29] J. Wang, B. Wylie-van Eerd, T. Sluka, C. Sandu, M. Cantoni, X.-K. Wei, A. Kvasov, L. J. McGilly, P. Gemeiner, B. Dkhil, A. Tagantsev, J. Trodahl, and N. Setter, *Nat. Mater.* **14**, 985 (2015).
  - [30] T. Gu, T. Scarbrough, Y. Yang, J. Íñiguez, L. Bellaiche, and H. J. Xiang, *Phys. Rev. Lett.* **120**, 197602 (2018).
  - [31] G. Kresse and J. Furthmüller, *Comp. Mater. Sci.* **6**, 15 (1996).
  - [32] G. Kresse and J. Furthmüller, *Phys. Rev. B* **54**, 11169 (1996).
  - [33] P. E. Blöchl, *Phys. Rev. B* **50**, 17953 (1994).
  - [34] J. P. Perdew, A. Ruzsinszky, G. I. Csonka, O. A. Vydrov, G. E. Scuseria, L. A. Constantin, X. Zhou, and K. Burke, *Phys. Rev. Lett.* **100**, 136406 (2008).
  - [35] X. Gonze and C. Lee, *Phys. Rev. B* **55**, 10355 (1997).
  - [36] J. C. Wojdeł and J. Íñiguez, *arXiv preprint arXiv:1312.0960* (2013).
  - [37] H. J. Xiang, M. Guennou, J. Íñiguez, J. Kreisel, and L. Bellaiche, *Phys. Rev. B* **96**, 054102 (2017).